Crystal Structure of the *Homo sapiens* Kynureninase-3-Hydroxyhippuric Acid Inhibitor Complex: Insights into the Molecular Basis Of Kynureninase Substrate Specificity†

Santiago Lima,[‡,⊥] Sunil Kumar,[§,⊥] Vijay Gawandi,[§] Cory Momany,[||] and Robert S. Phillips*[,‡,§]

Department of Biochemistry and Molecular Biology, University of Georgia, Athens, Georgia 30602, Department of Chemistry, University of Georgia, Athens, Georgia 30602, Department of Pharmaceutical and Biomedical Sciences, College of Pharmacy, University of Georgia, Athens, Georgia 30602

Received August 30, 2008

Homo sapiens kynureninase is a pyridoxal-5′-phosphate dependent enzyme that catalyzes the hydrolytic cleavage of 3-hydroxykynurenine to yield 3-hydroxyanthranilate and L-alanine as part of the tryptophan catabolic pathway leading to the de novo biosynthesis of NAD^+. This pathway results in quinolinate, an excitotoxin that is an NMDA receptor agonist. High levels of quinolinate have been correlated with the etiology of neurodegenerative disorders such as AIDS-related dementia and Alzheimer's disease. We have synthesized a novel kynureninase inhibitor, 3-hydroxyhippurate, cocrystallized it with human kynureninase, and solved the atomic structure. On the basis of an analysis of the complex, we designed a series of His-102, Ser-332, and Asn-333 mutants. The H102W/N333T and H102W/S332G/N333T mutants showed complete reversal of substrate specificity between 3-hydroxykynurenine and L-kynurenine, thus defining the primary residues contributing to substrate specificity in kynureninases.

In mammals, the essential amino acid L-tryptophan is a precursor for metabolites such as the neurotransmitter serotonin, the hormone melatonin, nicotinic acid, and NAD^+, with the latter two being the primary metabolic fate of dietary tryptophan. The catabolic cascade that leads to the de novo biosynthesis of nicotinic acid and NAD^+, commonly known as the kynurenine pathway,[1] is notable for intermediates with important neuroactive properties. Kynureninase, the third enzyme along the kynurenine pathway, is a pyridoxal-5′-phosphate (PLP)[a] dependent enzyme that catalyzes the hydrolytic cleavage of 3-hydroxy-L-kynurenine (3-OH-Kyn) to yield 3-hydroxyanthranilic acid and L-alanine (eq 1, R = OH). One further kynurenine pathway enzyme, 3-hydroxyanthranilate-3,4-dioxygenase, metabolizes 3-hydroxyanthranilic acid, the product of which undergoes a nonenzymatic rearrangement leading to the formation of quinolinate.[2] Quinolinate has endogenous neurotoxic activity[3] that is mediated via its agonist effect on glutamate sensitive NMDA ionotropic receptors,[4] and its excitotoxic effect has been correlated with the etiology of many neurodegenerative diseases including AIDS-related dementia,[5,6] Huntington's disease,[7,8] amyotrophic lateral sclerosis,[9] and Alzheimer's disease.[10,11] The increasing body of evidence implicating changes in normal concentrations of quinolinate in CNS tissues with neurotoxicity has led to the idea that altering the ratio of quinolinic acid to other kynurenine pathway metabolites could provide a neuroprotective effect during the onset of such maladies.[12−15] Thus, our goal was to provide a robust template that can be used for rational and in silico drug design as well as complex pharmacophore library screening. Herein we report the crystal structure of *Homo sapiens* kynureninase (HKynase) complexed with 3-hydroxyhippuric acid (**5**), a novel competitive inhibitor of kynureninase. The complex reveals important enzyme−ligand interactions that should be considered for the design and screening of novel kynureninase inhibitors.

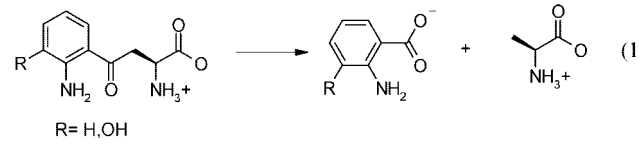

(1)

Two functional orthologues of kynureninase are known, a "constitutive", primarily eukaryotic enzyme[16] that preferentially catalyzes the hydrolysis of 3-OH-Kyn (eq 1, R = OH) and a primarily prokaryotic "inducible"[16] enzyme that catalyzes the hydrolysis of L-kynurenine (L-Kyn) to yield anthranilic acid and L-Ala (eq 1, R = H). Although both orthologues are able to catalyze the hydrolysis of their noncognate substrates, they do so at about 100-fold lower efficiency.[17,18] Indeed, a number of organisms, especially fungi, are known to contain both orthologues.[16] To date, the molecular basis of the substrate specificity that allows these enzymes to differentiate between their substrates has not been elucidated. Some insight into this mechanism was gained through docking studies with the native structure of *H. sapiens* kynureninase and 3-OH-L-Kyn as the target ligand.[18] These results revealed that two active site residues, His-102 and Asn-333, could play an important role in substrate binding and specificity.[18] We present herein additional experimental evidence supporting this hypothesis.

Results and Discussion

Synthesis of 5. Compound **5** was designed as an analogue of 3-OH-Kyn that would bind to HKynase and be stable during cocrystallization for up to several weeks. The synthesis of **5** started from readily available 3-hydroxybenzaldehyde (**1**), as shown in Scheme 1. After protection of the hydroxyl group in

† PDB accession code: 3E9K.

* To whom correspondence should be addressed. Phone: (706) 542-1996. Fax: (706) 542-9454. E-mail: rsphillips@chem.uga.edu. Address: Department of Chemistry, University of Georgia, Athens, GA 30602.

‡ Department of Biochemistry and Molecular Biology, University of Georgia.

§ Department of Chemistry, University of Georgia.

|| Department of Pharmaceutical and Biomedical Sciences, College of Pharmacy, University of Georgia.

⊥ S.L. and S.K. contributed equally to this work.

[a] Abbreviations: PLP, pyridoxal-5′-phosphate; L-Kyn, L-kynurenine; 3-OH-Kyn, 3-hydroxy-L-kynurenine; HKynase, *Homo sapiens* kynureninase; **5**, 3-hydroxyhippuric acid.

10.1021/jm8010806 CCC: $40.75
Published on Web 12/17/2008

Scheme 1

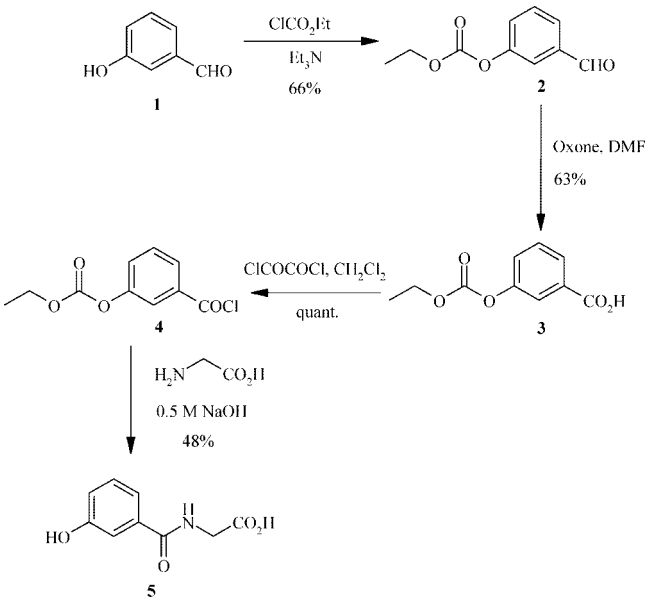

Scheme 2

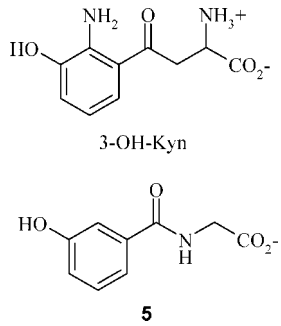

1 with ethylchloroformate to obtain 3-ethoxycarbonyloxybenzaldehyde (**2**), the aldehyde was oxidized to 3-ethoxycarbonyloxybenzoic acid (**3**) with oxone in DMF. The carboxylic acid (**3**) was then converted to 3-ethoxycarbonyloxybenzoyl chloride (**4**) with oxalyl chloride. Finally, deprotection of the hydroxyl group of **4** and formation of **5** was achieved in a single step by the reaction of **4** with glycine in the presence of 0.5 M sodium hydroxide. The product **5** is at least 98% pure based on HPLC and ^{1}H NMR (see Supporting Information).

Inhibition of Hkynase by 5. Our previous efforts to complex HKynase crystals with substrate and analogues had proven unsuccessful due to severe crystal cracking immediately upon exposure to the compounds in solution. Substituted hippurates were chosen for complexation because these compounds are structural analogues of L-Kyn/3-OH-Kyn (Scheme 2), which can form a Michaelis complex with HKynase. Because the hippurates do not have a free amino group, they bind without forming a covalent adduct with PLP, thus avoiding the structural rearrangements associated with substrate binding,[19] common among PLP-dependent aminotransferases, which can lead to crystal cracking during complexation. The parent compound, hippuric acid, does not show any detectable inhibition of HKynase at 1 mM. Of the other substituted hippurates tested, 2-amino-3-hydroxyhippuric acid (synthesis not shown) oxidizes rapidly in solution and thus could not be used in incubations to grow crystals. 2-Aminohippuric acid proved to be unsuitable because it also did not inhibit HKynase at a concentration of 1 mM. Compound **5** was the most stable inhibitor of the substituted hippurates tested and was thus chosen for the cocrystallization experiments. This compound was found to be a moderate competitive inhibitor of HKynase with a K_i of 60 μM. The fact that **5** is the most potent inhibitor of the compounds tested reflects the contribution of the 3-OH moiety to substrate specificity observed between kynurenine and 3-hydroxykynurenine among kynureninases.[18] Inhibitors that contain an α-amino group capable of forming an external aldimine with the PLP do not require the 3-OH to bind to HKynase because compounds such as 2-methoxybenzoylalanine[20] are also modest kynureninase inhibitors. However, the most potent inhibitor known for HKynase is 2-amino-4-[3′-hydroxyphenyl]-4-hydroxybutanoic acid, which contains both an α-amino group and the 3-OH, with a K_i value of 100 nM.[21]

Table 1. Summary of Crystallographic Analysis

data collection and processing statistics	
space group	*C*2
resolution range (outer shell), Å	89.09−1.65 (1.68−1.65)
no. of reflections (outer shell)	55449 (2096)
average $I/\sigma I$ (outer shell)	24.1 (1.9)
redundancy (outer shell)	3.5 (2.3)
completeness (outer shell), %	96.3 (68.4)
R_{merge} (outer shell)	0.050 (0.362)
refinement statistics	
R_{factor} (outer shell)	0.154 (0.251)[b]
R_{free}[a] (outer shell)	0.190 (0.342)
mean *B* value, Å^2	16.65
rmsd from ideal geometry	
bond angles, deg	1.067
bond distances, Å	0.007
Ramachandran plot residues in favored/allowed/disallowed regions, %	97.06/2.71/0.23

[a] R_{free} calculated with 5.1% of the total data that were excluded from refinement. [b] The outer shell resolution range used in refinement was 1.69−1.65 Å.

Human Kynureninase-5 Inhibitor Complex. Statistics for the refined model are presented in Table 1. The structure (PDB accession number 3E9K) contained one monomer per asymmetric unit and had good geometry with 441/1 residues in the allowed/disallowed regions of the Ramachandran plot. The final model was refined to an R_{value} of 0.152, R_{free} value of 0.189, and covers 96% of the predicted amino acid sequence with 669 water molecules included in the final structure. The biologically active unit (dimer) can be generated by applying the crystallographic symmetry operator 1-*x*, -*y*, -*z* to the monomer. The regions between residues 1−5, 377−387, and 461−465 could not be modeled due to poorly ordered electron density. These regions had disordered electron density in the native HKynase structure as well.[18] Electron density could be seen extending between the ε amino group of Lys-276 and the C-4′ of PLP, an observation consistent with a PLP internal aldimine covalent adduct. Positive density for the **5** molecule could be clearly observed in a difference electron density map ($F_o - F_c$) calculated from the unrefined molecular replacement solution. Upon docking the molecule of **5**, electron density for the atoms improved and became continuous (Figure 1). Further refinement revealed the presence of two water molecules, water 669 and water 671, in difference electron density maps within a short distance of the C2 atom of the aromatic ring of **5**. Refinement of these waters and compound **5** at full occupancy produced density for both molecules at negative contour levels in a difference electron density map. Upon adjustment of occupancies to 20% for water 669 and 671 and 80% for compound **5**, no residual positive or negative density ($<3\sigma$) could be observed for either molecule. Interestingly, water 669 occupies a position relative to **5** similar to that which would be occupied by a

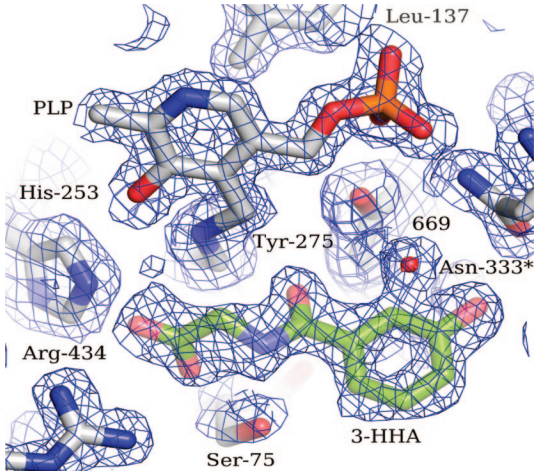

Figure 1. Electron density map showing continuous electron density for atoms of **5** (green carbon atoms, CPK coloring) in the active site of Hkynase.

substituent at the 2-position of the aromatic ring of **5**. Water 669 is stabilized by hydrogen bonds to the hydroxyl group of Tyr-275 (2.90 Å) and the δ NH_2 group of Asn-333* (3.19 Å) (* denotes residues on the 2-fold symmetry related monomer). Thus, this partial occupancy water molecule reveals some of the interactions that are likely to stabilize the 2-amino substituent on the aromatic ring in 3-OH-Kyn and L-Kyn.

The molecule of **5** is stabilized within the HKynase active site by interactions with residues from both monomer chains. The aromatic ring moiety of **5** lies in the active site pocket between the side chains of Ile-110*, His-102*, Tyr-275, Trp-305*, Phe-306*, Phe-314*, and Asn-333* (Figure 2). Trp-305* and Phe-314* stabilize **5** via alignment of their molecular quadrupole moments toward the aromatic ring (3.53 and 3.73 Å, respectively) and sandwich it with a π-stacking interaction against the side chain of His-102*. Trp-305 is strictly conserved in kynureninases of both eukaryotic and prokaryotic origin. Interestingly, Trp-305* also participates in cofactor binding by hydrogen bonding through its side chain pyrrole nitrogen with a PLP phosphate oxygen. Among PLP-dependent aminotransferases, the external aldimine scissile bond must be aligned perpendicular to the plane of the cofactor ring system in order to minimize the energy of the upcoming transition state.[22] Thus, maintaining the appropriate geometry between cofactor and substrate in order to maximize $\sigma-\pi$ overlap of the breaking bond with the cofactor π-system is crucial to catalysis. This complex reveals that Trp-305* likely plays a key role in maintaining the geometry of the external aldimine covalent adduct and subsequent intermediates by interacting with both substrate and cofactor. Moreover, Trp-305* is held firmly in position, relative to both cofactor and ligand, by two flanking quadrupole π-stacking interactions with the side chains of Phe-165 and Phe-306*. Phe-165 is a crucial active site residue because it participates in cofactor binding by π-stacking with the pyridine ring moiety of PLP. Phe-165 is stabilized in this position by one further quadrupole π-stacking interaction with the side chain of Phe-225. Phe-165, Trp-305*, and Phe-314* are strictly conserved among kynureninases regardless of their substrate specificity. Furthermore, all kynureninases have either a histidine or tryptophan residue at the bottom of the active site cavity to provide a π-stacking interaction to the substrate ring moiety.

Other interactions that stabilize **5** in the HKynase active site include hydrogen bonding between the 3-hydroxyl ring substituent and the side chain δ oxygen of Asn-333* (3.54 Å). Also, the carbonyl oxygen of **5** is involved in a weak hydrogen bond with the hydroxyl oxygen of Tyr-275 (3.77 Å) and the amide nitrogen of **5** is within hydrogen bonding distance to the Ser-75 γ oxygen (3.63 Å). On the other side of the active site cavity, and near the Lys-276-PLP internal aldimine imine bond, the carboxylate of **5** forms an ion pair with Arg-434 (2.98 and 3.06 Å), and hydrogen bonds with the ε nitrogen of His-253 (2.74 Å), and with the γ oxygen of Ser-75 (2.88 Å). The interaction between the carboxylate of **5** (which is equivalent to the α-carboxylate of L-enantiomer substrates) with the strictly conserved Arg-434 is well characterized among members of the PLP-dependent aspartate aminotransferase superfamily and is crucial to catalysis.[19,23,24]

A structural superposition of native (PDB accession code 2HZP) and **5** complexed HKynase reveals no major structural conformational changes. However, the side chains of residues Tyr-226, Arg-428, and Arg-434 showed conformational differences associated with the presence of **5**. Specifically, Arg-434 forms an electrostatic bond with the carboxylate oxygens of **5**. To do so, the Arg-434 guanidino nitrogens must move 7.7 Å from the position observed in native HKynase.[18] Consistent with the partial occupancy for **5**, the difference electron density map suggests two conformational states for the side chain of Arg-434: a high occupancy state (80%) in which the side chain interacts with the carboxylate oxygens of **5**, and a low occupancy state (20%) in which no ligand is present in the active site and the Arg-434 side chain conformation resembles that of native HKynase. Similarly, Tyr-226 and Arg-428 showed additional density in a difference electron density map, suggesting that these residues must adopt different conformations in order to accommodate **5** in the active site cavity. These residues were modeled to have 80% and 20% conformations as well. Interestingly, these residues do not directly contact ligand atoms, yet they line the surface of an interdomain channel that leads to the active site cavity. Thus, these residues appear to be dynamically involved in substrate binding by allowing access to the active site. The position of the side chains of these residues in ligand bound kynureninase places them at 4.4 Å (between hydroxyl oxygens of Tyr-226) and 3.7 Å (between guanidino nitrogens of Arg-428) from those in native HKynase.

The structure of the HKynase−**5** complex provides new insights into the catalytic mechanism of kynureninase. In previous studies on the mechanism of kynureninase from *Pseudomonas fluorescens*, we determined the stereochemistry of inhibition by transition state analogues and proposed that a general acid−base catalyst was involved in hydration of the substrate carbonyl and cleavage of the resulting *gem*-diol to give the carboxylic acid product.[25] The stereochemistry of inhibition by dihydrokynurenine and retro-aldol reactions catalyzed by kynureninase suggested that the water addition occurred from the *re*-face of the carbonyl.[25] In the present structure, the face of the inhibitor carbonyl equivalent to the *re*-face of the substrate is exposed, and the opposite face is covered by the ring of Tyr-275 and the side chain of Ser-75. Thus, the structure of the 5-HKynase complex is consistent with the stereochemistry of inhibition by dihydrokynurenine and suggests Tyr-275 may be an auxiliary acid−base catalyst for the reaction. Supporting the idea that Tyr-275 may play a critical role in catalysis is the observation that this Tyr residue is strictly conserved in all known kynureninase sequences (Figure 3). In addition, Ser-75 could potentially donate a hydrogen bond to the carbonyl, and it is also strictly conserved (Figure 3). A plausible mechanism for HKynase, taking into account the new structural data, is

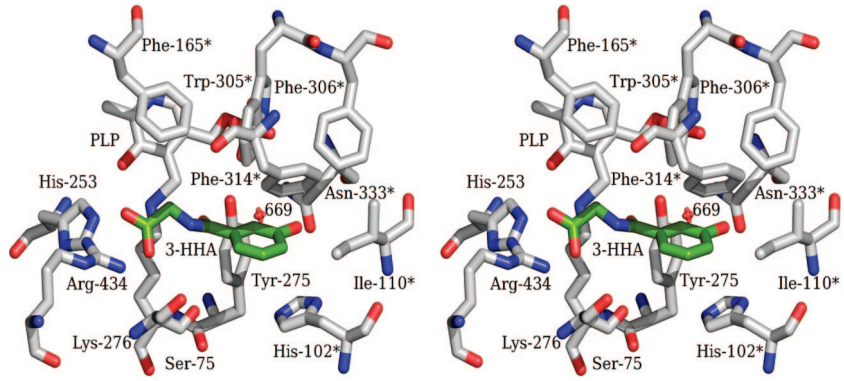

Figure 2. Relaxed-eye stereo representation of the binding interactions of **5** (colored green, ball and stick atoms) within the HKynase active site. Residues contributed from the symmetry related monomer are labeled with an asterisk (*).

Bacillus	IYLDGN**S**LGL	GIDG**W**TEGE.	N**Y**KYLNAGPG	AYQI**GT**PHVL
Clostridium	IYMDGN**S**LGL	AIKI**W**GVED.	S**Y**KYLNGGPG	GFLL**GT**HNMF
Pichia	IYLCGN**S**LGL	GVES**H**FNHPG	S**Y**KYLNSGPG	SYRQ**SN**PSVI
Saccharomyces	TYLCGN**S**LGL	AVES**H**FKHPE	S**Y**KYLNAGPG	GFRQ**SN**PSVI
Aspergillus	LYLCGN**S**LGL	GVTG**H**FVQHD	T**Y**KYLNSGPG	GFQL**SN**PSVL
Shewanella	LYFTGN**S**LGL	GVEG**H**FHAV.	T**Y**KYLNSSAG	GWQI**SN**APVM
Cytophaga	AYFCGH**S**LGL	GVEG**H**WKAA.	S**Y**KYLNGGPG	GFQV**SN**APVF
Myxococcus	VYLAGN**S**LGL	GVEG**H**HHGR.	S**Y**KYLNAGPG	GWQL**SN**PPIF
Stigmatella	VYLAGN**S**LGL	GVEG**H**FHAR.	S**Y**KYLNGGPG	GWQL**SN**PPIF
Acidobacteria	VYLVGH**S**LGL	GVEG**H**FRGK.	S**Y**KYLNGGPG	GWQL**SN**PSIL
Xanthomonas	TYLVGN**S**LGL	GVEG**H**FTGP.	N**Y**KYLNAGPG	GWQL**SN**PPVL
Human	IYFLGN**S**LGL	AAYG**H**EVGK.	S**Y**KYLNAGAG	GFRI**SN**PPIL
Dog	IYFSGN**S**LGL	GVYG**H**EVGK.	S**Y**KYLNSGAG	GFRI**SN**PPIL
Rat	IYFLGN**S**LGL	GAYG**H**EVGK.	S**Y**KYLNSGAG	GFRI**SN**PPIL
Mouse	IYFLGN**S**LGL	GAYG**H**DVGK.	S**Y**KYLNSGAG	GFRI**SN**PPIL
Chicken	IYFVGN**S**LGL	GVHG**H**FNGQ.	T**Y**KYLNSGAG	GFRL**SN**PPIL
Zebra fish	IYFAGN**S**LGL	GVHG**H**TEGS.	T**Y**KYMNSGAG	GFRL**SN**QPIL
Caenorhabditis	IYLCGN**S**LGL	GVFG**H**MSGE.	S**Y**KYGCTGAG	GYRI**SN**PPIH
Dictyostelium	IYLTGN**S**LGL	GVEG**H**HKGD.	T**Y**KYLNSGPG	GFRM**SN**PSVA
Pseudomonas	IYLDGN**S**LGA	LIRS**W**NTAG.	T**Y**KYLNGGPG	RYLC**GT**QPIT
Burkholderia	IYLDGN**S**LGA	LIRS**W**NTAG.	T**Y**KYLNGGPG	RFLC**GT**QPIV
Comamonas	IYLDGN**S**LGA	LITS**W**NKAG.	S**Y**KYLNGGPG	RYLC**GT**QPMI
Ralstonia	IYLDGN**S**LGA	LIRS**W**NDAD.	G**Y**KYLNGGPG	RMLT**GT**APQL
Oceanicola	VYMDGN**S**LGP	LITA**W**NRAG.	S**Y**KFLNGGPG	RMRV**GT**PPMI
Rhodobacter	IYLDGN**S**LGP	LITG**W**NRAG.	T**Y**KYLNSGPG	RMRV**GT**PPVI
Bradyrhizobium	IYLDGN**S**LGA	LIRG**W**NSAG.	T**Y**KYLNGGPG	RMRI**GT**PPII
Silicibacter	IYLDGN**S**LGP	LIKA**W**NTAD.	T**Y**KYFNGGPG	RLRV**GT**PSIV
Erythrobacter	IYLDGN**S**LGC	LIRS**W**NEAG.	G**Y**KYLCGGPG	QLQC**GT**SPVL
Arthrobacter	SYLDGN**S**LGR	LIRG**W**D.EE.	T**Y**KYLNGGPG	GFLS**GT**PAIF
	69 78	98 106	274 283	328 337

Figure 3. Sequence alignments of kynureninases from various organisms. Numbers at the bottom refer to the human sequence.

shown in Scheme 3. In the 3-OH-Kyn Schiff's base, Lys-276 removes the α-proton to form a quinonoid species, which is rapidly reprotonated at C-4′ to form a ketimine.[26] Lys-276 can then act as a general base to deprotonate a water molecule so that it can add to the carbonyl. A potential donor for the *gem*-diol of the reaction intermediate is water-657 hydrogen bonded to the side chain of Asp-426. We note that **5** is not quite positioned like a substrate would be because the α-hydrogen would have to be closer to Lys-276 for proton abstraction. The reaction of substrate with the PLP would likely result in reorganization of the active site bringing the catalytic residues into position. Interestingly, the complex shows that Tyr-275 also hydrogen bonds with the PLP phosphate, which suggests a possible involvement of its side chain in the catalytic cycle by mediating a proton transfer from the phosphate to the carbonyl. In this scenario, Tyr-275 could initiate $C_\gamma-C_\beta$ cleavage by deprotonation after formation of the *gem*-diol intermediate. The proposed mechanistic model resembles that of tyrosine phenol-lyase, where we found that Tyr-71 forms a hydrogen bond with the PLP phosphate in the internal aldimine and donates a proton to the phenol leaving group during catalysis.[27]

Kinetic Characterization of HKynase Mutants. The structure of **5** bound in the active site, shown in Figure 2, shows that Asn-333* accepts a hydrogen bond from the 3-OH of the bound ligand. As shown in the sequence alignments in Figure 3, the corresponding residue in bacterial kynureninase is a Thr. Characterization of the kinetic properties of the HKynase N333T mutant revealed a 9-fold decrease in k_{cat} for L-Kyn, but no change in K_m (Table 2). This mutant has weaker 3-OH-Kyn binding (6-fold higher K_m) and k_{cat} at least 1100 times slower

Scheme 3

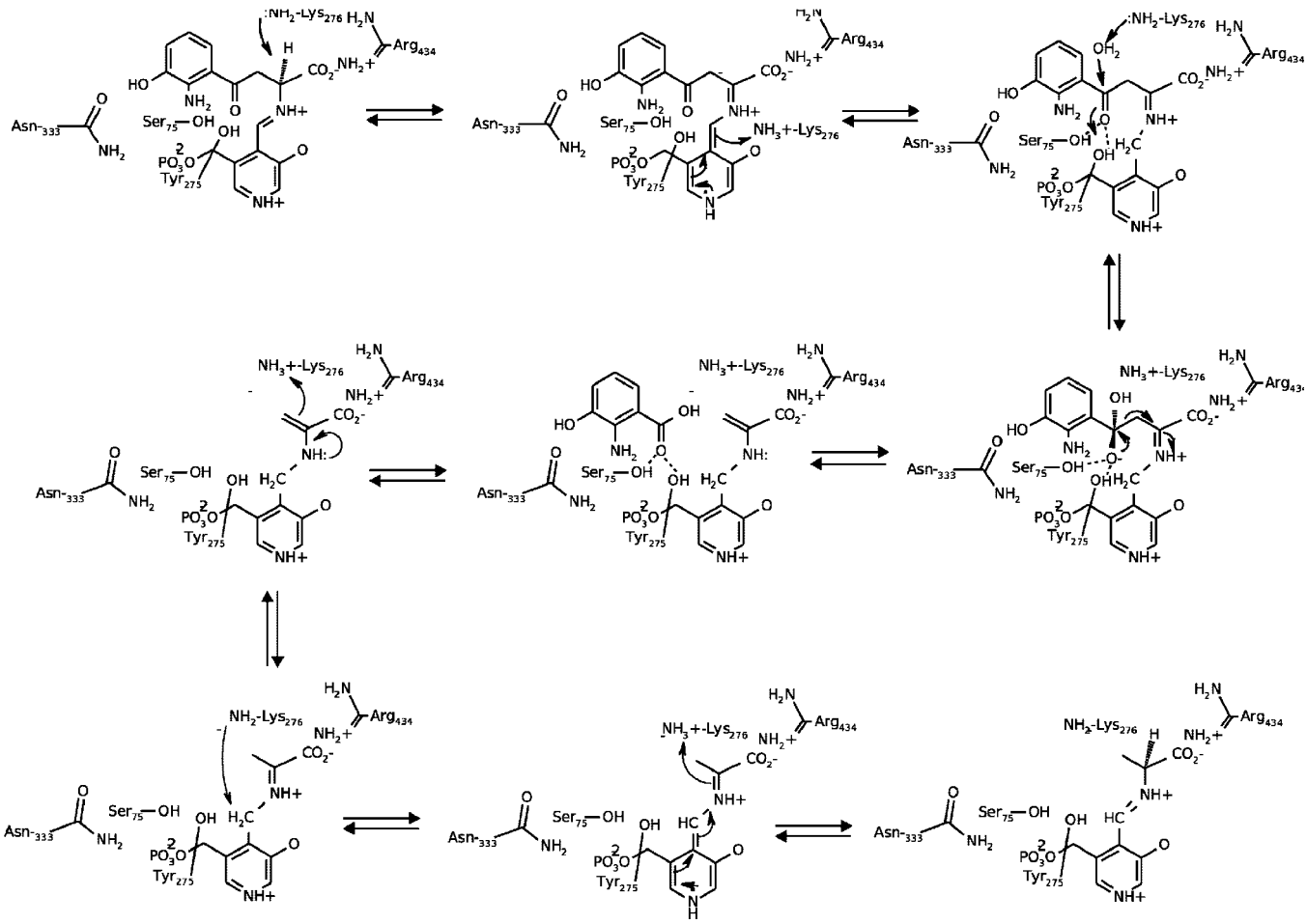

Table 2. L-Kynurenine and 3-OH-DL-Kynurenine Kinetic Constants for Wild Type and Mutant HKynases

	L-kynurenine			3-OH-DL-Kynurenine			L-Kyn/3-OH-DL-Kyn
enzyme	K_m (μM)	k_{cat} (s^{-1})	k_{cat}/K_m (M^{-1} s^{-1})	K_m (μM)	k_{cat} (s^{-1})	k_{cat}/K_m (M^{-1} s^{-1})	k_{cat}/K_m ratio
wild type	495	0.230	465	28.3	3.5	1.23×10^5	3.78×10^{-3}
N333T	499	0.026	52.1	>200	$<3.9 \times 10^{-3}$	19.8	2.6
S332G/N333T	540	0.017	31.4	>510	$<10.9 \times 10^{-3}$	21.5	1.5
H102W/N333T	327	0.007	21.4	N/A	N/A	<0.0165	$>1.36 \times 10^3$
H102W/S332G/ N333T	143	0.018	125.6	N/A	N/A	<0.0165	$>7.61 \times 10^3$

than wild type HKynase. Thus, this mutation affects 3-OH-Kyn binding and reduces its catalytic efficiency (k_{cat}/K_m) by a factor of more than 6×10^3, whereas the k_{cat}/K_m for L-Kyn is reduced only 9-fold. Hence, the hydrogen bond formed between the 3-OH group in 3-OH-Kyn and the carbonyl oxygen of Asn-333* appears to be an important determinant for the 3-OH-Kyn reaction. It is important to note that the K_m and V_{max} values of 3-OH-Kyn for N333T and S332G/N333T mutants could not be accurately determined, as rates for high concentrations of 3-OH-Kyn showed significant substrate inhibition. Thus, K_m values for N333T and S332G/N333T HKynase are estimated as greater than the highest 3-OH-Kyn concentration at which hydrolysis rates were still increasing in a linear fashion. The k_{cat}/K_m values for these mutants were calculated from the second-order rate constant obtained from the linear portion of a v vs [S] plot. Subsequently, the estimated K_m and calculated k_{cat}/K_m values were used to estimate the upper limit of k_{cat}. N333T and S332G/N333T mutant HKynases show a very slight preference for L-Kyn over 3-OH-Kyn (Table 2).

Isolation and characterization of H102W mutant HKynase was not possible because it could not be purified from the soluble cellular extract and appeared entirely in the insoluble protein fraction. We did not attempt to solubilize and refold protein from the inclusion bodies that resulted from these cultures. This protein in the insoluble pellet was of identical apparent SDS-PAGE molecular weight as wild-type HKynase. However, combination of the H102W and N333T mutations in the H102W/N333T double mutant restored the expression of soluble protein to levels similar to that of wild-type HKynase. These results are consistent with the observation that kynureninases contain pairings of residues at these positions that are consistently either His/Asn or Trp/Thr, as can be seen in Figure 3. Characterization of the HKynase mutant H102W/N333T revealed a small decrease in k_{cat} and K_m values for L-Kyn so that the k_{cat}/K_m value only decreases about 2.5-fold. However, the H102W/N333T mutant HKynase did not exhibit any measurable activity with 600 μM 3-OH-Kyn and 37.2 μM HKynase. Thus, these values were used to estimate a theoretical upper limit for k_{cat}/K_m by assuming 3-OH-Kyn $K_m \geq 600$ μM and $V_{max} \leq 0.0001$ absorbance min^{-1}, the minimal rate that could be measured. The net effect of the H102W/N333T double mutation is a decrease in catalytic efficiency toward 3-OH-Kyn

by a factor of at least 7.5×10^6 when compared to that of wild-type HKynase. Thus, removing the hydrogen bonding partner at the δ-position of Asn-333, increasing the local nonpolar environment, and introducing a large bulky side chain (Trp) at position 102 effectively act to exclude any 3-OH-Kyn binding at the concentrations measured. This suggests that residues Asn-333 and His-102 are the primary substrate specificity contacts for the 3-substituent on the kynurenine aromatic ring. Although the overall ratio of substrate specificity for 3-OH-Kyn/L-Kyn is reversed in the H102W/N333T mutant, this mutant is 22-fold less efficient at hydrolyzing L-Kyn than the wild-type enzyme. This suggests that a surrounding shell of residues contribute to catalytic efficiency. To further probe which residues contribute to catalytic efficiency, we introduced a third mutation, S332G, a residue showing a conserved pattern among orthologues utilizing L-Kyn or 3-OH-Kyn similar to that of His-102 and Asn-333 (Figure 3). In most 3-OH-Kyn hydrolyzing kynureninases, a Ser residue is conserved at this position, whereas the enzymes from organisms lacking the 3-OH-Kyn metabolite contain a conserved Gly (Figure 3). In the HKynase-**5** complex, Ser-332 does not form hydrogen bonds or have electrostatic contacts with any atoms of **5**. Yet, Ser-332 forms a hydrogen bond through the backbone amide nitrogen with one of the PLP phosphate oxygens. Characterization of the H102W/S332G/N333T triple mutant showed it has the strongest activity and catalytic efficiency toward L-Kyn of all Hkynase mutants studied. Furthermore, it showed no detectable activity with 3-OH-Kyn (Table 2) and has a 6-fold improvement in k_{cat}/K_m over the H102W/N333T mutant Hkynase. Thus, this mutation restores catalytic efficiency with L-Kyn to one-third of that measured with wild-type enzyme. In contrast, the S332G/N333T double mutant shows no improvement in k_{cat}/K_m over that measured in the N333T single mutant. From these results, we infer that the increased backbone flexibility provided by Gly-332 facilitates the interaction between Thr-333 and the bulky side chain of Trp-102, allowing a better fit of L-Kyn within the mutant active site cavity. This result suggests that two shells of residues surrounding the ligand atoms determine catalytic efficiency in kynureninases. One shell of residues directly contacts ligand atoms, providing essential acid/base, steric, and electrostatic interactions, and the other contributes remotely to the geometric arrangement of the active site and plays a dynamic role in catalysis. Interestingly, kynureninase from *Ralstonia metallodurans* was reported to have comparable activity with both L-Kyn and 3-OH-Kyn.[28] Yet, as shown in Figure 3, this kynureninase has an active site that contains the Trp/Gly/Thr pairing, further emphasizing the role played by outer shell residues in substrate specificity and catalysis. It will be of interest to use the HKynase H102W/S332G/N333T triple mutant for directed evolution experiments to identify residues remote from the active site which contribute to specificity and catalysis.

Currently, a number of kynureninase inhibitors have been reported in the literature.[20,21,25,29−33] Until now, their design has been based primarily on mechanistic considerations due to a lack of knowledge regarding the primary substrate binding mode and substrate−enzyme interactions required for in silico directed drug design. The HKynase−**5** complex reveals important restraints for the design and screening of novel substrate analogues and inhibitors. First, the following atoms should be designated as potential hydrogen bonding partners for ligand atoms: the side chain δ-oxygen of Asn-333*, the side chain hydroxyl oxygen of Tyr-275, and the γ-oxygen of Ser-75. Second, hydrophobic interactions should be maintained between aromatic substituents on screened ligands and the side chains of Ile-110*, Trp-305*, Phe-306*, and Phe-314*. HKynase−**5** interactions clearly show that a strong quadrupole molecular alignment occurs between the side chains of Trp-305*, Phe-314*, and the aromatic ring moiety of **5**, as well as ligand π-stacking against the side chain of His-102*. Third, electrostatic and/or hydrogen bonding interactions should be assigned between ligand atoms and the guanidino nitrogens of Arg-434 and the imidazole nitrogen atoms of His-253. Fourth, our results clearly show that His-102 and Asn-333 are the residues involved in substrate specificity for 3-OH-Kyn. As such, the interaction between these residues and ligand atoms should be used as a one of the primary forms of binding mode evaluation in docking studies. Furthermore, scoring of docked poses should consider the interaction between ligand atoms and Arg-434 side chain atoms as a strong indicator of acceptable docking because this form of stabilization is known to be crucial in ligand binding and stabilization throughout the PLP-dependent aspartate aminotransferase family of enzymes. Finally, we note that **5** is an ideal lead compound for combinatorial synthesis of libraries of possible HKynase inhibitors.

Experimental Section

Crystallization, Data Collection, and Molecular Replacement. Human kynureninase was expressed and purified as previously described.[18] Complexed kynureninase-3-hydroxyhippuric acid crystals were grown using the modified microbatch under oil technique at 25 °C by mixing (1:1 ratio) an HKynase solution (9 mg mL^{-1} in 50 mM HEPES, pH 5.1, and 0.1 mM PLP) with a crystallization solution containing 0.05 M $MgCl_2$, 0.1 M Tris (pH 8.0), 25% PEG 3000, and 350 μM **5**. Dark-yellow crystals appeared after 4−5 weeks and grew to dimensions of 0.075 mm × 0.05 mm × 0.015 mm. These crystals were flash frozen in liquid nitrogen with cryoprotectant containing 1 mM **5**, 55 mM $MgCl_2$, 110 mM Tris (pH 8), 33% PEG 3000. These crystals had space group *C*2 with cell constants $a = 74.44$ Å, $b = 77.12$ Å, $c = 94.55$ Å, $\beta = 109.35$. X-ray synchrotron data were collected ($\lambda = 1.007$ Å, 200 frames, 1° oscillations) at the Advanced Photon Source beamline 19-ID and were processed and scaled with HKL3000.[34] The merged SCALEPACK[34] intensities were used as input for the molecular replacement program Phaser[35] using the HKynase (PDB accession code 2HZP) (HKynase) coordinates as the phasing model. All water, hetero, and PLP coordinates were deleted from the input model. The molecular replacement solution and Hkynase−**5** complex were refined with Refmac5.[36] Water addition was done with ARP/wARP.[37] The PLP cofactor and compound **5** were manually introduced with COOT.[38] TLS[39] refinement was performed with the following groups: 6−37, 38−45, 46−120, 121−190, 191−213, 214−357, 358−375, 376−412, 413−460. The model of **5** and library description were created with the CCP4i Monomer Library Sketcher.[40] Molprobity[41] was used to evaluate the quality of the final model.

Inhibition Kinetics. Compound **5** was evaluated for its ability to inhibit the reaction of HKynase with its cognate substrate, 3-OH-Kyn. Assays were performed by following the absorbance change at 370 nm as 3-OH-Kyn (DL mixture, USBiochemical Corp.) is converted to 3-hydroxyanthranilic acid and L-Alanine ($\Delta\varepsilon = -4500$ M^{-1} cm^{-1}) with a Cary 1 UV/visible spectrophotometer equipped with a Peltier temperature controlled cell 6 × 6 cell compartment. Assays contained 30 mM potassium phosphate, pH 8.0, and 40 μM PLP at 37 °C together with variable amounts of 3-OH-Kyn and four different concentrations of **5**. Data were fit to a competitive inhibition model with Cleland's COMPO program.[42]

Site Directed Mutagenesis. Mutants were created using the QuickChange site-directed mutagenesis kit (Stratagene). The following mutants were created and sequenced to confirm the desired codon change: H102W, N333T, S332G/N333T (double mutant), H102W/N333T (double mutant), H102W/S332G/N333T (triple mutant). The mutagenesis primers used were (only coding strand

written, mutated bases bold underlined): H102W: 5′-CCA AAA TAG CAG CCT ATG GT**T GG**G AAG TGG GGA AGC GTC CTT GG-3′; S332G/N333T: 5′-GGG GTC TGT GGA TTC CGA ATT **GGC** A**CC** CCT CCC ATT TTG TTG GTC-3′; N333T: 5′-GTC TGT GGA TTC CGA ATT TCA A**CC** CCT CCC ATT TTG TTG G-3′.

Synthesis of 3-Hydroxyhippuric Acid (5). 3-Ethoxycarbonyloxybenzaldehyde (2).[43] 3-Hydroxybenzaldehyde (1; 15.0 g, 0.123 mol) was dissolved in 100 mL dry pyridine, cooled to 4 °C, and ethyl chloroformate (20 mL) was added dropwise over a period of 30 min. The resulting solution was stirred for 2 h at room temperature. The solvent was evaporated in vacuo, and water (150 mL) was added to the residue. The product was extracted into ether, and the extract was washed consecutively with water, 5% HC1, 5% cold NaOH, and again with water. The dried organic extract was evaporated in vacuo to give a dark-red viscous product (15.5 g, 65%). ^{1}H NMR (400 MHz, $CDCl_3$) δ 1.29 (t, 3H), 4.21 (m, 2H), 7.96 (dd, 1H), 7.57 (d, 1H), 7.72 (d, 1H), 7.74 (m, 1H), 9.61 (s, 1H).

3-Ethoxycarbonyloxybenzoic acid (3).[44] 3-Ethoxycarbonyloxybenzaldehyde (6 g, 0.03 mol) was dissolved in 30 mL DMF. Oxone (19 g, 0.03 mol) was added, and the mixture was stirred at room temperature for 3 h. The reaction was monitored by TLC and, after completion, 1 N HCl was added to dissolve the salts. The crude product was extracted into ethyl acetate (50 mL), the organic extract washed with 1N HCl (3 × 15 mL), brine (2 × 10 mL), and then dried over Na_2SO_4. Evaporation of the solvent in vacuo gave 3-ethoxycarbonyloxybenzoic acid (**3**), which was purified by silica gel column chromatography (60:40 EtOAc/hexane). Yield, 3.86 g (63%). ^{1}H NMR (400 MHz, $CDCl_3$) δ 1.29 (t, 3H), 4.21 (m, 2H), 7.93 (dd, 1H), 7.63 (d, 1H), 8.02 (d, 1H), 8.06 (m, 1H), 12.54 (s, 1H).

3-Ethoxycarbonyloxybenzoyl chloride (4). To 3.0 g (0.15 mol) of 3-ethoxycarbonyloxybenzoic acid in dry dichloromethane, one equiv of 0.2 M oxalyl chloride in dichloromethane was added dropwise, and the mixture was stirred for 5 h at room temperature. The crude 3-methoxycarbonyloxybenzoyl chloride (2.35 g, 68%) was obtained after evaporation of excess solvent and reagent. ^{1}H NMR(400 MHz, $CDCl_3$) δ 1.29 (t, 3H), 4.21 (m, 2H), 7.93 (dd, 1H), 7.66 (d, 1H), 7.96 (d, 1H), 8.00 (m, 1H).

3-Hydroxyhippuric acid (5).[45] The finely powdered 3-ethoxycarbonyloxybenzoyl chloride (1.7 g, 0.007 mol) was added to 0.6 g of glycine in 20 mL of 0.5 N NaOH. Subsequently, 1N NaOH was continuously added to the solution over a period of 15 min to maintain the pH above 10. The reaction mixture was then acidified with conc. HCl, and **5** was extracted with ethyl acetate (3 × 15 mL). The organic extracts were dried and evaporated, and the crude product was recrystallized from 50% ethanol−water. Yield, 0.8 g (48.3%), mp 184−187 °C. ^{1}H NMR (DMSO-d_6) δ 3.87 (d, 2H, CH_2), 6.88−6.91 (m, 3H, Ar−H), 7.21−7.25 (m, 1H, Ar−H), 8.68 (t, 1H, NH), 9.60 (s, 1H, OH), 12.60 (s, 1H, CO_2H). MS, anion mode, direct injection ESI $(M - H)^- = 194.0$ (100%); $(2M - H)^- = 389.2$ (36%).

Acknowledgment. Results shown in this report are derived from work performed at Argonne National Laboratory, Structural Biology Center at the Advanced Photon Source. Argonne is operated by University of Chicago Argonne, LLC, for the U.S. Department of Energy, Office of Biological and Environmental Research under contract DE-AC02-06CH11357. Use of the Advanced Photon Source was supported by the U.S. Department of Energy, O. o. S., Office of Basic Energy Sciences, under contract no. W-31-109-Eng-38.

Supporting Information Available: ^{1}H NMR, MS, and HPLC of **5**. This material is available free of charge via the Internet at http://pubs.acs.org.

References

(1) Soda, K.; Tanizawa, K. Kynureninases: enzymological properties and regulation mechanism. *Adv. Enzymol. Relat. Area Mol. Biol.* **1979**, *49*, 1–40.
(2) Colabroy, K. L.; Begley, T. P. The pyridine ring of NAD is formed by a nonenzymatic pericyclic reaction. *J. Am. Chem. Soc.* **2005**, *127*, 840–841.
(3) Schwarcz, R.; Whetsell, W. O., Jr.; Mangano, R. M. Quinolinic acid: an endogenous metabolite that produces axon-sparing lesions in rat brain. *Science* **1983**, *219*, 316–318.
(4) Stone, T. W.; Perkins, M. N. Quinolinic acid: a potent endogenous excitant at amino acid receptors in CNS. *Eur. J. Pharmacol.* **1981**, *72*, 411–412.
(5) Heyes, M. P.; Brew, B.; Martin, A.; Markey, S. P.; Price, R. W.; Bhalla, R. B.; Salazar, A. Cerebrospinal fluid quinolinic acid concentrations are increased in acquired immune deficiency syndrome. *Adv. Exp. Med. Biol.* **1991**, *294*, 687–690.
(6) Achim, C. L.; Heyes, M. P.; Wiley, C. A. Quantitation of human immunodeficiency virus, immune activation factors, and quinolinic acid in AIDS brains. *J. Clin. Invest.* **1993**, *91*, 2769–2775.
(7) Heyes, M. P.; Swartz, K. J.; Markey, S. P.; Beal, M. F. Regional brain and cerebrospinal fluid quinolinic acid concentrations in Huntington's disease. *Neurosci. Lett.* **1991**, *122*, 265–269.
(8) Giorgini, F.; Moller, T.; Kwan, W.; Zwilling, D.; Wacker, J. L.; Hong, S.; Tsai, L. C.; Cheah, C. S.; Schwarcz, R.; Guidetti, P.; Muchowski, P. J. Histone deacetylase inhibition modulates kynurenine pathway activation in yeast, microglia, and mice expressing a mutant huntingtin fragment. *J. Biol. Chem.* **2008**, *283*, 7390–7400.
(9) Guillemin, G. J.; Meininger, V.; Brew, B. J. Implications for the kynurenine pathway and quinolinic acid in amyotrophic lateral sclerosis. *Neurodegener. Dis.* **2005**, *2*, 166–176.
(10) Leonard, B. E. Inflammation, depression and dementia: are they connected. *Neurochem. Res.* **2007**, *32*, 1749–1756.
(11) Guillemin, G. J.; Brew, B. J.; Noonan, C. E.; Takikawa, O.; Cullen, K. M. Indoleamine 2,3 dioxygenase and quinolinic acid immunoreactivity in Alzheimer's disease hippocampus. *Neuropathol. Appl. Neurobiol.* **2005**, *31*, 395–404.
(12) Stone, T. W.; Mackay, G. M.; Forrest, C. M.; Clark, C. J.; Darlington, L. G. Tryptophan metabolites and brain disorders. *Clin. Chem. Lab. Med.* **2003**, *41*, 852–859.
(13) Schwarcz, R.; Pellicciari, R. Manipulation of brain kynurenines: glial targets, neuronal effects, and clinical opportunities. *J. Pharmacol. Exp. Ther.* **2002**, *303*, 1–10.
(14) Stone, T. W.; Addae, J. I. The pharmacological manipulation of glutamate receptors and neuroprotection. *Eur. J. Pharmacol.* **2002**, *447*, 285–296.
(15) Tankiewicz, A.; Pawlak, D.; Buczko, W. Enzymes of the kynurenine pathway. *Postepy. Hig. Med. Dosw.* **2001**, *55*, 715–731.
(16) Shetty, A. S.; Gaertner, F. H. Kynureninase-Type enzymes of *Penicillum roqueforti*, *Aspergillus niger*, *Rhizopus stolonifer*, and *Pseudomonas fluorescens*: further evidence for distinct kynureninase and hydroxykynureninase activities. *J. Bacteriol.* **1975**, *122*, 235–244.
(17) Toma, S.; Nakamura, M.; Tone, S.; Okuno, E.; Kido, R.; Breton, J.; Avanzi, N.; Cozzi, L.; Speciale, C.; Mostardini, M.; Gatti, S.; Benatti, L. Cloning and recombinant expression of rat and human kynureninase. *FEBS Lett.* **1997**, *408*, 5–10.
(18) Lima, S.; Khristoforov, R.; Momany, C.; Phillips, R. S. Crystal structure of *Homo sapiens* kynureninase. *Biochemistry* **2007**, *46*, 2735–2744.
(19) Jager, J.; Moser, M.; Sauder, U.; Jansonius, J. N. Crystal structures of *Escherichia coli* aspartate aminotransferase in two conformations. Comparison of an unliganded open and two liganded closed forms. *J. Mol. Biol.* **1994**, *239*, 285–305.
(20) Chiarugi, A.; Carpenedo, R.; Molina, M. T.; Mattoli, L.; Pellicciari, R.; Moroni, F. Comparison of the neurochemical and behavioral effects resulting from the inhibition of kynurenine hydroxylase and/or kynureninase. *J. Neurochem.* **1995**, *65*, 1176–1183.
(21) Walsh, H. A.; Leslie, P. L.; O'Shea, K. C.; Botting, N. P. 2-Amino-4-[3′-hydroxyphenyl]-4-hydroxybutanoic acid; a potent inhibitor of rat and recombinant human kynureninase. *Bioorg. Med. Chem. Lett.* **2002**, *12*, 361–363.
(22) Dunathan, H. C. Conformation and reaction specificity in pyridoxal phosphate enzymes. *Proc. Natl. Acad. Sci. U.S.A.* **1966**, *55*, 712–716.
(23) Delle Fratte, S.; Iurescia, S.; Angelaccio, S.; Bossa, F.; Schirch, V. The function of arginine 363 as the substrate carboxyl-binding site in *Escherichia coli* serine hydroxymethyltransferase. *Eur. J. Biochem.* **1994**, *225*, 395–401.
(24) Almo, S. C.; Smith, D. L.; Danishefsky, A. T.; Ringe, D. The structural basis for the altered substrate specificity of the R292D active site mutant of aspartate aminotransferase from E. coli. *Protein Eng.* **1994**, *7*, 405–412.

(25) Dua, R.; Phillips, R. S. Stereochemistry and mechanism of aldol reactions catalyzed by kynureninase. *J. Am. Chem. Soc.* **1991**, *113*, 7385–7388.
(26) Phillips, R. S.; Sundararaju, B.; Koushik, S. V. The Catalytic Mechanism of Kynureninase from *Pseudomonas fluorescens*: Evidence for Transient Quinonoid and Ketimine Intermediates from Rapid-scanning Stopped-flow Spectrophotometry. *Biochemistry* **1998**, *37*, 8783–8789.
(27) Chen, H. Y.; Demidkina, T. V.; Phillips, R. S. Site-directed Mutagenesis of Tyrosine-71 to Phenylalanine in *Citrobacter freundii* Tyrosine Phenol-lyase: Evidence for Dual Roles of Tyrosine 71 as a General Acid Catalyst in the Reaction Mechanism and in Cofactor Binding. *Biochemistry* **1995**, *34*, 12276–12283.
(28) Kurnasov, O.; Goral, V.; Colabroy, K.; Gerdes, S.; Anantha, S.; Osterman, A.; Begley, T. P. NAD biosynthesis: identification of the tryptophan to quinolinate pathway in bacteria. *Chem. Biol.* **2003**, *10*, 1195–1204.
(29) Dua, R. K.; Taylor, E. W.; Phillips, R. S. *S*-Aryl-L-cysteine *S*,*S*-Dioxides: Design and evaluation of a new class of mechanism based inhibitors of kynureninase. *J. Am. Chem. Soc.* **1993**, *115*, 1264–1270.
(30) Walsh, H. A.; O'Shea, K. C.; Botting, N. P. Comparative inhibition by substrate analogues 3-methoxy- and 3-hydroxydesaminokynurenine and an improved 3 step purification of recombinant human kynureninase. *BMC Biochem.* **2003**, *4*, 13.
(31) Heiss, C.; Anderson, J.; Phillips, R. S. Differential effects of bromination on substrates and inhibitors of kynureninase from *Pseudomonas fluorescens*. *Org. Biomol. Chem.* **2003**, *1*, 288–295.
(32) Fitzgerald, D. H.; Muirhead, K. M.; Botting, N. P. A comparative study on the inhibition of human and bacterial kynureninase by novel bicyclic kynurenine analogues. *Bioorg. Med. Chem.* **2001**, *9*, 983–989.
(33) Carpenedo, R.; Chiarugi, A.; Russi, P.; Lombardi, G.; Carla, V.; Pellicciari, R.; Mattoli, L.; Moroni, F. Inhibitors of kynurenine hydroxylase and kynureninase increase cerebral formation of kynurenate and have sedative and anticonvulsant activities. *Neuroscience* **1994**, *61*, 237–243.
(34) Otwinowski, Z.; W., M. Processing of X-ray Diffraction Data Collected in Oscillation Mode. *Methods Enzymol.* **1997**, *276*, 307–326.
(35) McCoy, A. J.; Grosse-Kunstleve, R. W.; Storoni, L. C.; Read, R. J. Likelihood-enhanced fast translation functions. *Acta Crystallogr., Sect. D: Biol. Crystallogr.* **2005**, *61*, 458–464.
(36) Murshudov, G. N.; Vagin, A. A.; Dodson, E. J. Refinement of macromolecular structures by the maximum-likelihood method. *Acta Crystallogr., Sect. D: Biol. Crystallogr.* **1997**, *53*, 240–255.
(37) Lamzin, V. S.; Perrakis, A.; Wilson, K. S. The ARP/WARP suite for automated construction and refinement of protein models. In *International Tables for Crystallography, Volume F*; Kluwer Academic Publishers: Dordrecht, The Netherlands, 2001.
(38) Emsley, P.; Cowtan, K. Coot: model-building tools for molecular graphics. *Acta Crystallogr., Sect, D: Biol. Crystallogr.* **2004**, *60*, 2126–2132.
(39) Winn, M. D.; Isupov, M. N.; Murshudov, G. N. Use of TLS parameters to model anisotropic displacements in macromolecular refinement. *Acta Crystallogr., Sect. D: Biol. Crystallogr.* **2001**, *57*, 122–133.
(40) Collaborative Computational Project, N. The CCP4 Suite: Programs for Protein Crystallography *Acta Crystallogr., Sect. D: Biol. Crystallogr.* **1994**, *50*, 760−763.
(41) Davis, I. W.; Leaver-Fay, A.; Chen, V. B.; Block, J. N.; Kapral, G. J.; Wang, X.; Murray, L. W.; BryanArendall, W., III.; Snoeyink, J.; Richardson, J. S.; Richardson, D. C. MolProbity: all-atom contacts and structure validation for proteins and nucleic acids. *Nucleic Acids Res.* **2007**, *35*, W375–W383.
(42) Cleland, W. W. Statistical analysis of enzyme kinetic data. *Methods Enzymol.* **1979**, *63*, 103–138.
(43) Dalgliesh, C. E.; Mann, F. G. Synthesis of β-(3,4-dihydroxyphenyl)-*N*-methylserine (adrenalinecarboxylic acid). *J. Chem. Soc.* **1947**, 658–662.
(44) Travis, B. R. S., M.; Hollist, G. O.; Borhan, B. Facile Oxidation of Aldehydes to Acids and Esters with Oxone. *Org. Lett.* **2003**, *5*, 1031–1034.
(45) Acheson, R. M. B. D. A.; Brettle, R.; Harris, A. M. Synthesis of some acylglycines and related oxazolones. *J. Chem. Soc.* **1960**, 3457–3461.

JM8010806